Eur. Phys. J. Special Topics **208**, 39–52 (2012)

DOI: 10.1140/epjst/e2012-01605-4

THE EUROPEAN PHYSICAL JOURNAL SPECIAL TOPICS

Review

Anisotropic resonant X-ray scattering: Beauty of forbidden reflections

J. Kokubun[1,a] and V.E. Dmitrienko[2]

[1] Faculty of Science and Technology, Tokyo University of Science, Noda, Chiba 278-8510, Japan
[2] A.V. Shubnikov Institute of Crystallography, 119333 Moscow, Russia

Received 29 December 2011 / Received in final form 23 March 2012
Published online 15 June 2012

Abstract. Experimental results and their theoretical explanation are reviewed for fundamentals of anisotropic resonant X-ray scattering. Resonant scattering depends on X-ray polarization, i.e. the scattering reflects anisotropic environment of atoms in crystal. The polarization anisotropy in atomic scattering can excite the *forbidden* Bragg reflections. Studying this type of forbidden reflections we can distinguish electronic orbitals of specific symmetry. This method is very useful for studying local electronic states in crystal. We reveal detailed property of the anisotropic scattering, effect of quadrupole transition, thermal motion, magnetic scattering and so on. Especially successful examples are given in detail: observation of phase of the scattering factor, the hybridization of states with different parity, local chirality of atom in centrosymmetric crystals, thermal-motion-induced resonant reflections, etc.

1 Introduction

Resonant X-ray scattering essentially depends on X-ray polarization as well as energy. This fact means that the scattering is sensitive to orientation of unoccupied electronic orbitals as well as the density of state. In this case we should treat the atomic scattering factor as tensor quantity with respect to the components of X-ray polarization. Even for atoms of the same site in crystal, the scattering amplitudes are different if the atomic environments, i.e. interatomic directions, are different. Therefore conventional extinction rules for the *forbidden* Bragg reflections, related with glide-planes and/or screw-axes, can be violated in the resonant regions, and we can observe those reflections. We usually neglect the X-ray polarization anomaly in the experiment because the anisotropic term is generally very small compared with isotropic terms corresponding to mainly charge scattering. Observing the forbidden reflections, however, we can detect exclusively the anisotropic scattering term. Moreover, the resonant scattering factor is enhanced near the absorption edge. Therefore from the resonant forbidden reflections we can obtain the information about only the anisotropic part of the electronic states of resonant atoms.

[a] e-mail: kokubun@ph.noda.tus.ac.jp

The polarization anisotropy is also observed in absorption experiment (XANES). The phenomena such as linear dichroism and birefringence are closely related with the anisotropic scattering, but those methods are not flexible in comparison with the forbidden reflection experiment. In some sense, the information obtained from forbidden reflections is complimentary to XANES, where we see absorption coefficient averaged (summarized) over a unit cell: quite the contrary, the structure factor of forbidden reflection is proportional to differences of atomic factors of resonant atoms. Using the diffraction method we can realize very precise and highly technical experiment for probing local electronic states. Typical data of the diffraction experiment are azimuth dependence and energy spectrum of the scattering intensity. X-ray polarization analysis of the forbidden reflections gives more detailed information. Additionally different contributions to the atomic scattering tensors can be obtained from different forbidden Bragg reflections. Therefore we can distinguish specific tensor elements by control of many experimental conditions. From these measurements we can deduce important details about the nature of the resonant electronic states. Of course the synchrotron radiation, which has continuous energy and high brilliant and polarized X-rays, is indispensable for such experiment.

The electric dipole approximation, i.e. the first order approximation, is usually applied to the resonant X-ray scattering; this scattering is based on dipole-dipole (d-d also called E1E1) transition process, which depends on only X-ray polarization vectors. In higher order approximations, the resonant scattering also depends on X-ray wave vectors; the scattering process can be quadrupole-quadrupole (q-q, E2E2), dipole-quadrupole (d-q, E1E2), etc. The quadrupole effect is generally small compared with the d-d scattering but it can be observed in practice. Near K-absorption edge, according to selection rules for electronic orbitals, we can detect p-like states from the dipole transition, d-like states from the quadrupole transition and p-d hybridization of states from the d-q transition.

Templeton and Templeton [1] observed X-ray linear dichroism by synchrotron radiation experiment and Petcov et al. [2] observed birefringence as well as the dichroism with a technique like visible-light experiment. In 1982, Templeton and Templeton [3] observed also nonforbidden reflections intensities dependent on X-ray polarization and supposed that a special type of forbidden reflections can be excited owing to the polarization anisotropy. This polarization effect is caused by electric anisotropy of resonant atoms near the absorption edge. From these results it was pointed [4,5] out that the atomic scattering factor should be treated as tensor and traditional extinction rules for Bragg reflections were violated. In practice the forbidden reflections were observed in many crystals, first by Templeton and Templeton [6,7], Kirfel et al. [8] and then by many other groups. Even in cubic crystals the polarization anisotropy was observed with diffraction method [3,8]. In most cases, the observed azimuth dependence of the reflections was explained by the dipole approximation, e.g. in $NaBrO_3$ [6,7], Cu_2O, TiO_2 [8], FeS_2 [9], Fe_3O_4 [10], $HoFe_2$ [11], etc. In iron pyrite, FeS_2, the polarization anomaly of the forbidden reflections was directly studied with polarization analysis [9], and its property was also explained in the dipole approximation.

However, the forbidden reflections that are not allowed in dipole approximation were observed in some crystals. Finkelstein et al. [12] investigated the 111 forbidden rhombohedral reflection in hematite, α-Fe_2O_3, near the Fe K-absorption edge. The azimuthal dependence of the reflection was found to be sixfold, which was explained by q-q scattering. Templeton and Templeton [13] observed forbidden reflections in germanium crystal near the Ge K-edge at room temperature. Their properties were explained by d-q scattering. After that time Kirfel et al. [14] found d-q scattering in addition to d-d scattering from magnetite, Fe_3O_4, near the Fe K-edge. Kokubun et al. [15] measured the detailed energy spectra of the forbidden reflections in iron

pyrite. As a result different spectra were carefully examined in the pre-edge region of the Fe atom and their azimuthal dependence was explained by the d-d and q-q scattering combination [16]. Similar quadrupole effects were also reported in other crystals: spinel ferrites [17–19], TiO_2 [20], etc.

Considering the physics of forbidden reflection, a new type of anisotropic resonant scattering that is induced by atomic thermal motion was predicted [21,22]. In germanium crystal, the forbidden reflection was indeed strongly dependent on temperature and this result revealed that the large part of the intensity was caused by thermal-motion-induced (TMI) resonant scattering [23]. The Ge atoms are in regular tetrahedral symmetry, but the atomic displacement from the equilibrium position degrades the symmetry. Therefore thermal motion allows us to observe the anisotropic d-d scattering despite of high average site symmetry. The TMI scattering is mainly caused by the effect of optical phonon mode and additionally reflects thermal motion correlations. Other physical problems solved with the help of the resonant forbidden reflections are discussed in Sect. 4.

In this paper we introduce typical and remarkable experimental results on the forbidden reflections caused by the resonant anisotropy. We show also additional and complicated physical phenomena concerning resonant scattering, in particular, we consider the influence of the magnetic scattering, thermal motion and so on. It is demonstrated that the quadrupole scattering effect is typical of many crystals.

2 Basic theory

According to the second-order perturbation theory of interaction between photon and electronic states, the anomalous scattering factor near the absorption edge is given by

$$f_{\mathrm{Res}} = \frac{1}{m}\sum_n \frac{\langle a \,|\, (\boldsymbol{\varepsilon}' \cdot \boldsymbol{p})\, e^{-i\,\boldsymbol{k}'\cdot\boldsymbol{r}} \,|\, n\rangle \,\langle n \,|\, (\boldsymbol{\varepsilon} \cdot \boldsymbol{p})\, e^{i\,\boldsymbol{k}\cdot\boldsymbol{r}} \,|\, a\rangle}{E_a \;-\; E_n + \hbar\omega - i\Gamma_n/2}, \tag{1}$$

where $\boldsymbol{\varepsilon}$ and $\boldsymbol{k}$ represent the polarization and the wave vector of incident X-rays, and $\boldsymbol{\varepsilon}'$ and $\boldsymbol{k}'$ those of scattered X-rays, respectively. Equation (1) has a resonant denominator for X-ray energy $\hbar\omega$ from the ground state $|a\rangle$ of energy E_a to intermediate states $|n\rangle$ of energy E_n and width Γ_n. By expanding the exponential factor in Eq. (1), we obtain the approximation of the power series,

$$e^{i\,\boldsymbol{k}\cdot\boldsymbol{r}} \approx 1 + i\boldsymbol{k}\cdot\boldsymbol{r}. \tag{2}$$

Therefore, the atomic scattering factor containing non-resonant terms for the i-th atom in the unit cell can be expanded in a series over the wave vectors $\boldsymbol{k}$ and $\boldsymbol{k}'$:

$$\begin{aligned}(\hat{f}_i)_{jk} = {} & f_i^0\delta_{jk} + (\hat{f}_i^{dd})_{jk} + i(\hat{f}_i^{dqs})_{jkl}(k_l - k'_l) \\ & + i(\hat{f}_i^{dqa})_{jkl}(k_l + k'_l) + (\hat{f}_i^{qq})_{jklm}k_l k'_m + (\hat{f}_i^{mag})_{jk},\end{aligned} \tag{3}$$

where f_i^0 is the conventional Thomson scattering factor given by a scalar quantity, $\hat{f}_i^{dd}$and $\hat{f}_i^{qq}$ describe dipole-dipole (d-d) and quadrupole-quadrupole (q-q) scattering whereas $(\hat{f}_i^{dqs})_{jkl} = (\hat{f}_i^{dqs})_{kjl}$ and $(\hat{f}_i^{dqa})_{jkl} = -(\hat{f}_i^{dqa})_{kjl}$ correspond to symmetric and antisymmetric (relative to the first two indices) contributions to mixed dipole-quadrupole (d-q) scattering, and $\hat{f}_i^{mag}$ stands for magnetic scattering, which should be added in the case of magnetic material. The d-d scattering factor is the tensor of second rank, the d-q factors of third rank and the q-q factor of fourth rank [24–27].

Using the tensorial scattering factor $\hat{f}_i$, the tensorial crystal structure factor is given by

$$\hat{F}(\boldsymbol{G}) = \sum_i \hat{f}_i e^{-2\pi\, i\boldsymbol{G}\cdot\boldsymbol{r}_i}, \tag{4}$$

where $\boldsymbol{G}$ is the scattering vector and $\boldsymbol{r}_i$ is the atomic coordinate of the i-th atom in the unit cell; the tensors $\hat{f}_i$ of crystallographically equivalent atoms are related by the space-group operations. The scattering matrix for the 3×3 format of a structure factor $\hat{F}$ is described as

$$\hat{M} = \begin{pmatrix} M_{\sigma'\sigma} & M_{\sigma'\pi} \\ M_{\pi'\sigma} & M_{\pi'\pi} \end{pmatrix} = \begin{pmatrix} \boldsymbol{\sigma}'\,\hat{F}\,\boldsymbol{\sigma} & \boldsymbol{\sigma}'\,\hat{F}\,\boldsymbol{\pi} \\ \boldsymbol{\pi}'\,\hat{F}\,\boldsymbol{\sigma} & \boldsymbol{\pi}'\,\hat{F}\,\boldsymbol{\pi} \end{pmatrix}, \tag{5}$$

and the total scattering intensity, I, for the σ-polarized incident X-rays is given by

$$I = I_{\sigma'} + I_{\pi'} = |M_{\sigma'\sigma}|^2 + |M_{\pi'\sigma}|^2, \tag{6}$$

where $\boldsymbol{\sigma}$ and $\boldsymbol{\pi}$ represent the two polarization vectors of incident X-rays, and $\boldsymbol{\sigma}'$ and $\boldsymbol{\pi}'$ those of scattered X-rays, respectively.

3 Experimental

In this paper we treat mainly compounds of 3d transition metals near their K-absorption edges. Our synchrotron radiation experiments were mainly performed with a four-circle diffractometer installed on beam line 4C at Photon Factory, KEK in Tsukuba, Japan. The incident X-ray energy was selected with a double Si (111) monochromator which was detuned to about 60% intensity yield in order to exclude higher harmonic components. We used a reflection plane that is parallel to surface of the studied single crystal.

The samples were mounted on the diffractometer with measured reflection plane perpendicular to φ axis of the diffractometer. On this condition we can easily make azimuthal angle scanning. We set additionally a polarization analyzer on 2θ arm of the diffractometer if we need polarization analysis of the scattered X-rays. The other experimental arrangements were typical of a diffraction experiment with synchrotron radiation. Since the polarization of the incident X-rays was in the horizontal plane and the scattering plane was vertical, the incident beam was σ polarized. The energy dependence and the azimuth dependence of the forbidden reflections were obtained from integrated intensity with θ–2θ scan. Of course, we subtract the background intensity from the scan. Here we must take care of contribution of Renninger reflections (multiple-wave peaks), which are excited via nonforbidden reflections and observed in the azimuthal scanning. We first measured the Renninger plot and made azimuthal correction by comparing with the calculation. Then we searched flat positions between those peaks and selected carefully the azimuthal angles to avoid the Renninger effect at each energy. This procedure allows us to obtain smooth data with the intrinsic symmetry.

4 Results and discussion

We first present a simple structure case, iron pyrite FeS_2 [9,15,16], which is a cubic crystal with the space group $Pa\bar{3}$. The iron atoms occupy the *fcc* positions and the site symmetry is $\bar{3}$. In this symmetry the d-d and q-q scattering are allowed, but

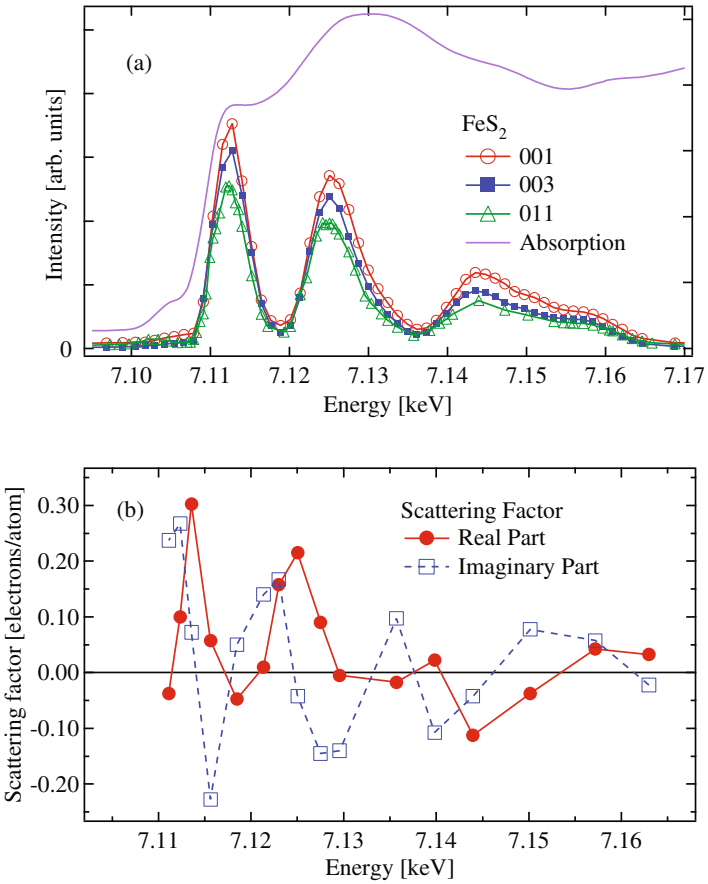

Fig. 1. Observed energy spectra in iron pyrite, FeS_2, near the Fe K-absorption edge: (a) the absorption coefficient and forbidden reflections intensities [15]; (b) the real and imaginary parts of the anisotropic tensor element of the iron scattering factor [32].

the d-q scattering is not allowed by inversion symmetry. We need only one complex parameter (the difference of atomic X-ray susceptibilities along and perpendicular to the corresponding threefold axis) to explain the d-d forbidden reflections intensities in iron pyrite [15]. Figure 1(a) shows the observed energy spectra of the forbidden reflections intensities near the Fe K-absorption edge. The absorption data were measured in advance by usual XAFS technique with a powder sample. In order to distinguish the scattering character, d-d or q-q scattering, we must perform the azimuthal scanning or more complicated measurement, e.g. polarization analysis. Above the edge, the shapes of energy spectra are almost the same as shown in Fig. 1(a). The azimuth dependence well agrees with the calculation of d-d scattering at the energies above the edge [9,15]. The results of polarization analysis of the scattering X-rays are also in good agreement with the dipole calculation [9]. Therefore we conclude that the reflections above the edge are caused by the d-d scattering from p-like states. The derived scattering factor depicted in Fig. 1(b) is discussed later.

In the pre-edge region, on the other hand, the shape of the energy spectrum is different from each other as shown in Fig. 2(a). Even for the same reflection, spectra change with azimuth angle. These results indicate that other contributions in addition to the d-d scattering factor are involved in the scattering. In fact the azimuth

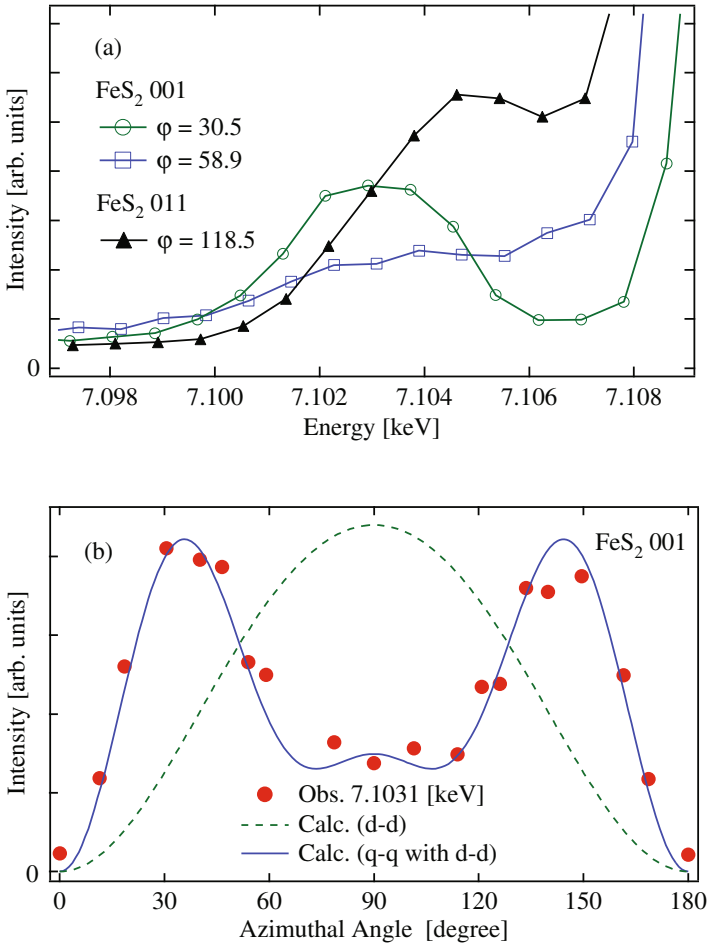

Fig. 2. Forbidden reflections intensities in the Fe pre-edge region of FeS_2. (a) Observed energy spectra of the 001 and 011 forbidden reflections at different azimuthal angles, φ. (b) Azimuthal angle dependence of the 001 reflection. The dashed curve in (b) is calculated based on the d-d scattering. The solid curve denotes the d-d and q-q mixed calculation. (The observed 001 and 011 data are the same as in references [16] and [15], respectively.)

dependence well agrees with the calculation of d-d and q-q mixed scattering as shown in Fig. 2(b). Therefore we conclude that the scattering in the pre-edge region has d-d and q-q mixed character.

Similar situation is also seen in tetragonal rutile crystal, TiO_2 [8,20]. The d-d and q-q scattering is also allowed in the crystal. Above the Ti K edge the character of the forbidden reflections is explained by the d-d scattering. In the pre-edge region, however, the energy spectra show different profiles and the azimuth dependence is quite different from the d-d calculation [20]. Figure 3 shows the azimuth dependences of the forbidden reflection at two energies above and below the edge. The azimuth dependence at the lowest resonant energy nearly coincides with the q-q calculation. Thus in the pre-edge region of the 3d transition metals the q-q scattering is large in comparison with the d-d scattering.

In magnetite, Fe_3O_4 [10,14,17,18,28,29], the Fe atoms occupy two different sites, tetrahedral and octahedral sites. In this case the scattering conditions at the sites are

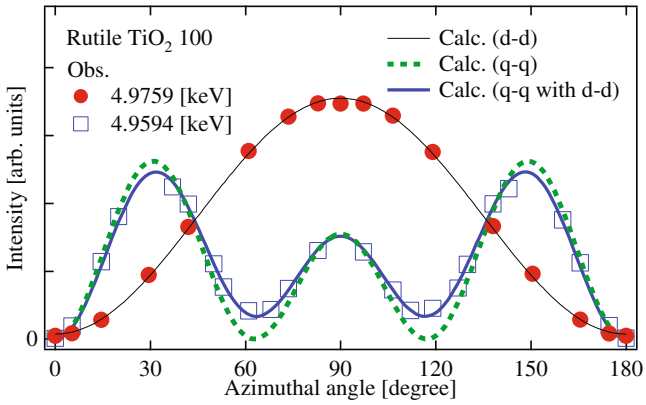

Fig. 3. Observed azimuthal angle dependence of the 100 forbidden reflection intensity in rutile, TiO_2, above the Ti K-absorption edge (4.9759 [eV]) and at the lowest resonant energy (4.9594 [eV]) in the pre-edge region. The curves denote the d-d and/or q-q scattering calculations. (All observed data are the same as in Ref. [20].)

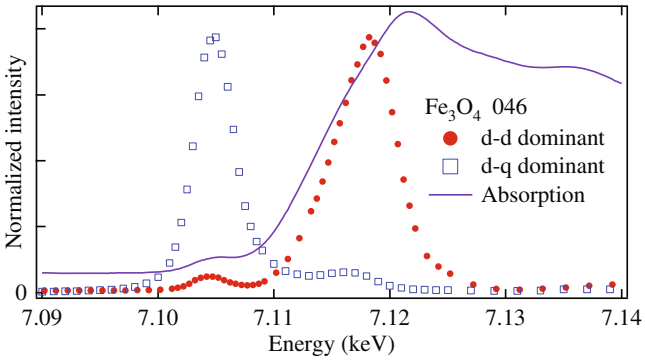

Fig. 4. Energy spectra of the 046 forbidden reflection intensity in Fe_3O_4 near the Fe K-absorption edge with polarization analyzer. Circles and squares were observed on special experimental conditions, fixed azimuthal angles and polarization angles. Circles (squares) are on the conditions where the d-q (d-d) scattering almost vanishes. (All data are not published before, though the tentative results are in Ref. [29].)

rather complicated. Because of symmetry restrictions, for the tetrahedral site only d-q scattering gives contribution to forbidden reflections, whereas d-d and q-q scatterings (and not d-q) are allowed from the octahedral site. In the forbidden reflection experiment both the d-d and the d-q scatterings have been observed near the Fe K edge though evidence of the q-q scattering is absent until now. It is generally difficult to measure separately different characters of the scattering. However the experimental conditions for their observations are different. By selecting the appropriate reflection plane and azimuthal angle and using polarization analyzer we can measure separately the d-d or d-q scattering from magnetite [29]. The observed energy spectra are shown in Fig. 4. The one of them (squares) shows the d-q scattering from almost hybridized p-d mixed states of the tetrahedral site. Another spectrum (circles) shows the d-d scattering from almost p-like states of the octahedral site.

For the energy spectra of the anisotropic d-d scattering we measured three crystals. Figure 5 shows the observed energy spectra of iron, cobalt and nickel pyrites, FeS_2, CoS_2, NiS_2 [30], which have the same pyrite structure. As shown in this

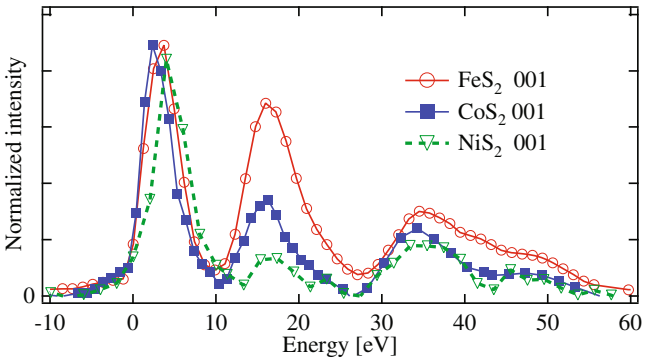

Fig. 5. Energy spectra of the 001 forbidden reflection intensities in three pyrite crystals, FeS_2, CoS_2, NiS_2 (same data as in Ref. [30]). The origin of the energy scale denotes each metal K-absorption edge.

figure the similar spectra are observed from the similar crystals above the metals K-absorption edges. The reason may be that in high-energy region the spectra are mainly determined by surrounding sulfur atoms, because all metal ions have the same divalent states.

In addition to the anisotropic scattering intensity we can measure the phase of the scattering factor. When allowed multiple Bragg reflections are excited simultaneously with forbidden reflections, the strong Renninger peaks are observed in the azimuthal scanning of the forbidden reflection. The Renninger scattering amplitude has opposite phase in each side of the reflection peak, therefore the interference effect with the anisotropic scattering is different in each side. By means of the interference we can determine the phase of anisotropic scattering factor because the amplitude of the Renninger reflection can be calculated if the crystal structure is known.

Using this technique we can obtain separately the real and imaginary parts of the atomic scattering factor, i.e. two separate energy spectra. For details of the multiple-wave interference theory for forbidden reflections and the phase determination method, see references [31] and [32] respectively (see also [33–37] and references therein). Figure 1(b) shows the successfully obtained energy spectra of real and imaginary parts of the iron pyrite scattering factor. The observed spectra are supported by the electronic states calculations with muffin-tin and full potential approach. The refined calculated spectra are in good agreement with the observation [32]. The separately obtained real and imaginary spectra could be very useful for studying the details of the electronic states. This is more informative than only the intensity data.

We next take a rare case, anatase crystal [38], where the resonant scattering from only p-d hybridized orbitals with different parity can be observed. Anatase is a tetragonal polymorph of TiO_2, the Ti site symmetry is $\bar{4}m2$. In the crystal, all d-d and q-q atomic scattering factors of Ti atoms are exactly the same. Therefore, in the forbidden reflections, we can observe only the d-q scattering. In this case two parameters are needed for the 002 forbidden reflection. Figure 6 shows the observed energy spectra of the reflection intensity. The shapes of the two spectra are almost identical at different temperatures. The shapes of azimuth dependences were also not changed by temperature. A little intensity increase was observed down to 20 K from room temperature (inset in Fig. 6), but the temperature dependence can be explained by usual Debye-Waller factor. Therefore we conclude that the observed anisotropic resonant scattering is almost pure d-q scattering induced by p-d hybridization of orbitals. This result is quite different from that in germanium crystal, which is largely

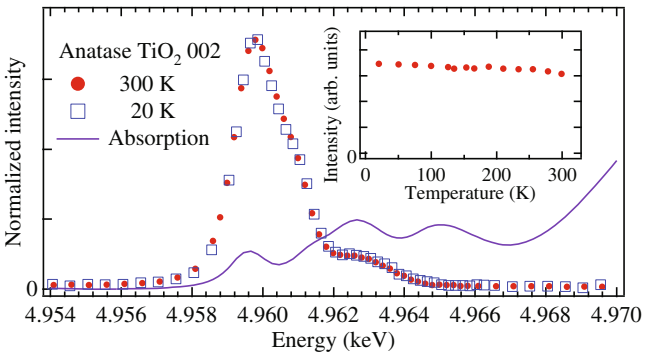

Fig. 6. Energy spectra of the anatase 002 forbidden reflection intensity measured at different temperatures near the Ti K-absorption edge. The spectra are normalized to a common maximum intensity. The inset shows the temperature dependence at the peak-top energy. (All data are the same as in Ref. [38].)

dependent on temperature, see below. A possible physical reason of this difference is that in anatase, contrary to germanium, the main contribution arises from the *antisymmetric* d-q term which cannot be induced by thermal motion of atoms. In spite of the same chemical formula, TiO_2, the property of the anisotropic resonant scattering is quite different in three polymorphs, rutile, anatase and brookite [26]. This reason is attributed to the different crystal structures and different site symmetries of Ti. We can observe only the anisotropic part of the resonant scattering and the allowed multi-pole contributions to scattering are restricted by the site symmetry. Therefore unfortunately we cannot select freely the scattering from specific electronic states.

We next consider magnetic effect on the resonant anisotropic scattering, and local chirality of atom in a centrosymmetric crystal. Hematite, α-Fe_2O_3 [12,39], has corundum structure of rhombohedral crystal, the Fe site symmetry is 3. For the forbidden reflections in hematite, d-d scattering is not allowed but d-q and q-q scatterings are allowed. In addition to the electric scattering the magnetic scattering can also affect the forbidden reflections because hematite has anti-ferromagnetic structure. In fact the non-resonant magnetic scattering was observed in hematite, though its intensity was much smaller than that of the resonant scattering. The observed forbidden 111 and 333 reflections in the crystal revealed one resonant peak only in the pre-edge energy region of the Fe atom. Figure 7 shows the observed azimuth dependence of the 111 and 333 forbidden reflections intensity at the resonant energy. The azimuth dependence of the 111 reflection shows almost threefold symmetry. This result is well explained by the interference between d-q and q-q scatterings. The crystal is centrosymmetric but the iron site have no inversion symmetry and the d-q contribution to the forbidden reflections depends on *antisymmetric* part of the third-rank tensor of the iron atomic susceptibility (remind that just the antisymmetric part is responsible for the effects of natural chirality in non-centrosymmetric crystals). Therefore the observation of d-q scattering in the 111 reflection is evidence of local chirality of the Fe atom.

On the other hand, the resonant 333 reflection in hematite shows complicated azimuth dependence, nearly mirror symmetry. This result is well explained by interference of non-resonant magnetic scattering with the d-q and q-q resonant electric scatterings. Resonant magnetic scattering can also bring similar contribution to the 333 reflection, but the effect is inconsistent with other experimental results. Namely clear evidence of the resonant magnetic scattering was not found. From these results it

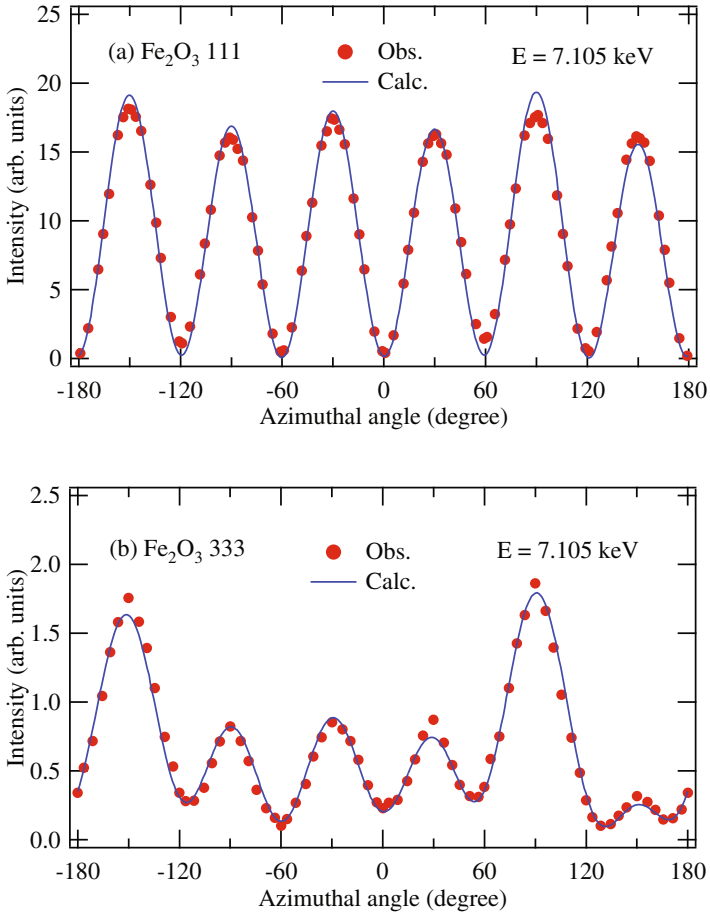

Fig. 7. Azimuthal angle dependence in hematite [39]: (a) the 111 and (b) the 333 reflections at the resonant energy near the Fe K pre-edge. The solid curves are calculated from a combination of the d-q, q-q resonant electric scatterings and non-resonant magnetic scattering. In the 111 reflection the electric scatterings are dominant.

is shown that the non-resonant magnetic scattering has a significant influence on the resonant electric scattering though its intensity is much smaller. Thus the interference between the magnetic and electric scatterings plays a very important role in hematite forbidden reflections. This phenomenon opens new ways for studying additional details of the magnetic structure, for instance, it allows us to determine the sign of the Dzyaloshinskii-Moriya interactions in this class of antiferromagnetics with weak ferromagnetism [40,41]. Very recently the sign has been really measured for another weak antiferromagnetic, $FeBO_3$ [42], using interference between resonant q-q scattering and non-resonant magnetic scattering. Moreover, in non-centrosymmetric MnSi crystal, it is possible to measure this way different components of the Dzyaloshinskii-Moriya vector never measured before [43].

The polarization properties of resonant forbidden reflections provide a direct way to distinguish right and left enantiomorphs of crystals [4,5]. The structure factors and corresponding intensities of the screw-axis forbidden reflections in right-handed and left-handed crystals are very different for right and left circular polarizations even in pure d-d approximation. Only recently this was experimentally confirmed for low quartz [44] (SiO_2, Si K-edge), berlinite [45] ($AlPO_4$, P K-edge), $CsCuCl_3$ [46]

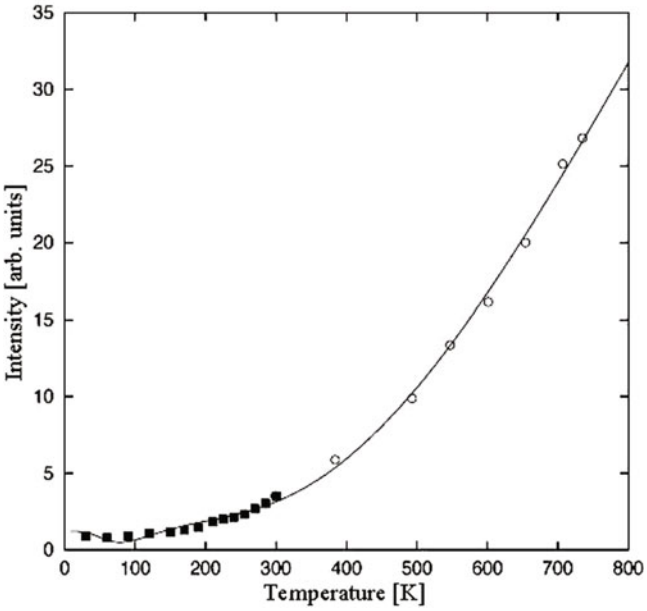

Fig. 8. Temperature dependence of the Ge 006 forbidden reflection intensity at the resonant energy near the Ge K-absorption edge [23,49]. The curve is calculated from the Einstein model for optical phonons with the thermal motion correlation considered.

(Cu K-edge), and tellurium [47] (Te L_1-edge) crystals (see also the paper of Tanaka [48] in this issue).

We finally consider the thermal-motion-induced contribution to forbidden reflections. Germanium crystal [13,23,49] has the diamond structure and the atomic site symmetry is $\bar{4}3m$. For this symmetry the d-d scattering factor is isotropic, therefore the forbidden reflections cannot be allowed in dipole approximation. Therefore the observed forbidden reflections should originate in other reasons. Figure 8 shows the temperature dependence of the forbidden 006 reflection intensity at the resonant energy near the Ge K edge. As shown in this figure the intensity strongly increases with temperature. From this result and the azimuth dependence we conclude that about 1/4 intensities at room temperature are pure d-q scattering but the other 3/4 intensities are caused by thermal-motion-induced (TMI) resonant scattering. By only the azimuth dependence we cannot know weather the scattering is caused by pure d-q or TMI scattering because the both azimuth dependences are completely the same. It is remarkable in the TMI scattering that the great enhancement of the intensity is observed in high temperature region. Furthermore information of the thermal motion correlation was derived from the TMI scattering in germanium [49]. The TMI scattering at a forbidden reflection has been also observed in other crystals, ZnO [50] and GaN [51]. Theoretical simulations show that the TMI scattering is mainly caused by the optical phonon mode [52]. Therefore the TMI scattering can give a new method for studying the phonon property in crystal.

We cannot review in this short paper other interesting and sometimes controversial phenomena studied via beautiful shine of forbidden reflections: a possible orbital ordering vs. the Jahn-Teller distortions in $LaMnO_3$ [34,35,53,54], charge ordering vs. atomic displacements during the Verwey transition in magnetite [55–57], recent observation of orbital currents in CuO crystals [58] and extremely small atomic

displacements in multiferroics [59] (see also numerous references therein). The forbidden reflections are also used very successfully in soft X-ray region near L- or M-edges [60].

5 Conclusion

Above we have presented only a small part of works dealing with forbidden reflections in resonant regions near X-ray absorption edges. Using forbidden reflections we have exclusively detected the information about local anisotropy of X-ray susceptibility of resonant atoms. This experimental technique is a very sensitive and useful method to study the local electronic states. In pyrite crystal, we have obtained separately the real and imaginary energy spectra of the anisotropic scattering factor by phase determination method and compared this result with different type of theoretical simulations. We have studied not only the dipole resonant scattering but also the quadrupole effects in many crystals because the quadrupole effects can be clearly seen this way compared with other experimental methods. The dipole-quadrupole and quadrupole-quadrupole scattering amplitudes are more sensitive to the specific details of local electronic states (for instance, to hybridization of orbitals with different parity). We can observe even the local chirality at the atomic scale. The method of forbidden reflection is also useful for studying the magnetic properties of crystals including tiny effects related with the Dzyaloshinskii-Moriya interaction. Furthermore, TMI resonant scattering can give a new opportunity to study the phonon displacements and the thermal motion correlations of atoms.

We are grateful to M. Blume and K. Ishida for their permanent passion for forbidden reflections encouraging us in our common work.

References

1. D.H. Templeton, L.K. Templeton, Acta Crystallogr. Sect. A **36**, 237 (1980)
2. A. Petcov, A. Kirfel, K. Fischer, Acta Crystallogr. Sect. A **46**, 754 (1990)
3. D.H. Templeton, L.K. Templeton, Acta Crystallogr. Sect. A **38**, 62 (1982)
4. V.E. Dmitrienko, Acta Crystallogr. Sect. A **39**, 29 (1983)
5. V.E. Dmitrienko, Acta Crystallogr. Sect. A **40**, 89 (1984)
6. D.H. Templeton, L.K. Templeton, Acta Crystallogr. Sect. A **41**, 133 (1985)
7. D.H. Templeton, L.K. Templeton, Acta Crystallogr. Sect. A **42**, 478 (1986)
8. A. Kirfel, A. Petcov, K. Eichhorn, Acta Crystallogr. Sect. A **47**, 180 (1991)
9. T. Nagano, J. Kokubun, I. Yazawa, T. Kurasawa, M. Kuribayashi, E. Tsuji, K. Ishida, S. Sasaki, T. Mori, S. Kishimoto, Y. Murakami, J. Phys. Soc. Jpn. **65**, 3060 (1996)
10. K. Hagiwara, M. Kanazawa, K. Horie, J. Kokubun, K. Ishida, J. Phys. Soc. Jpn. **68**, 1592 (1999)
11. S.P. Collins, D. Laundy, A. Stunault, J. Phys. Condens. Matter **13**, 1891 (2001)
12. K.D. Finkelstein, Q. Shen, S. Shastri, Phys. Rev. Lett. **69**, 1612 (1992)
13. D.H. Templeton, L.K. Templeton, Phys. Rev. B **49**, 14850 (1994)
14. A. Kirfel, T. Lippmann, W. Morgenroth, HASYLAB Annual Report 1995, Part II, p. 371
15. J. Kokubun, T. Nagano, M. Kuribayashi, K. Ishida, J. Phys. Soc. Jpn. **67**, 3114 (1998)
16. J. Kokubun, M. Kanazawa, K. Ishida, Photon Factory Act. Rep. 1998, Part B **16**, 13 (1999)
17. J. Garcia, G. Subias, M.G. Proeitti, H. Renevier, Y. Joly, J.L. Hodeau, J. Brasco, M.C. Sanchez, J.F. Ferau, Phys. Rev. Lett. **85**, 578 (2000)
18. M. Kanazawa, K. Hagiwara, J. Kokubun, K. Ishida, J. Phys. Soc. Jpn. **71**, 1765 (2002)

19. G. Subias, J. Garcia, M.G. Proietti, J. Blasco, H. Renevier, J.L. Hodeau, M.C. Sanchez, Phys. Rev. B **70**, 155105 (2004)
20. H. Sawai, J. Kokubun, K. Ishida, Photon Factory Act. Rep. 2002, Part B **20**, 122 (2003)
21. V.E. Dmitrienko, E.N. Ovchinnikova, K. Ishida, Pis'ma Zh. Eksp. Teor. Fiz. **69**, 885 (1999)
22. V.E. Dmitrienko, E.N. Ovchinnikova, K. Ishida, JETP Lett. **69**, 938 (1999)
23. J. Kokubun, M. Kanazawa, K. Ishida, V.E. Dmitrienko, Phys. Rev. B **64**, 073203 (2001)
24. M. Blume, in Resonant Anomalous X-Ray Scattering, edited by G. Materlik, C.J. Sparks, K. Fisher (Elsevier, Amsterdam, 1994), p. 495
25. S.W. Lovesey, E. Balcar, K.S. Knight, J. Fernandez-Rodrigues, Phys. Rep. **411**, 233 (2005)
26. V.E. Dmitrienko, K. Ishida, A. Kirfel, E.N. Ovchinnikova, Acta Crystallogr. Sect. A **61**, 481 (2005)
27. S.P. Collins, S.W. Lovesey, E. Balcar, J. Phys. Condens. Matter **19**, 213201 (2007)
28. J. Kokubun, M. Kawana, K. Ishida, Photon Factory Act. Rep. 2005, Part B **23**, 136 (2006)
29. J. Kokubun, M. Kawana, K. Ishida, Photon Factory Act. Rep. 2007 Part B **25**, 109 (2008)
30. J. Kokubun, K. Ishida, J. Crystallogr. Soc. Jpn. **44**, 161 (2002) (in Japanese)
31. J. Kokubun, K. Ishida, V.E. Dmitrienko, J. Phys. Soc. Jpn. **67**, 1291 (1998)
32. J. Kokubun, K. Ishida, D. Cabaret, F. Mauri, R.V. Vedrinskii, V.L. Kraizman, A.A. Novakovich, E.V. Krivitskii, V.E. Dmitrienko, Phys. Rev. B **69**, 245103 (2004)
33. T.L. Lee, R. Felici, K. Hirano, B. Cowie, J. Zegenhagen, R. Colella, Phys. Rev. B **64**, 201316 (2001)
34. R. Colella, Q. Shen, Acta Cryst. A**62**, 459 (2006)
35. Q. Shen, I.S. Elfimov, P. Fanwick, Y. Tokura, T. Kimura, K. Finkelstein, R. Colella, G.A. Sawatzky, Phys. Rev. Lett. **96**, 246405 (2006)
36. E.Kh. Mukhamedzhanov, M.M. Borisov, A.N. Morkovin, A.A. Antonenko, A.P. Oreshko, E.N. Ovchinnikova, V.E. Dmitrienko, Pis'ma Zh. Eksp. Teor. Fiz. **86**, 896 (2007)
37. E.Kh. Mukhamedzhanov, M.M. Borisov, A.N. Morkovin, A.A. Antonenko, A.P. Oreshko, E.N. Ovchinnikova, V.E. Dmitrienko, JETP Letters **86**, 783 (2007)
38. J. Kokubun, H. Sawai, M. Uehara, N. Momozawa, K. Ishida, A. Kirfel, R.V. Vedrinskii, N.M. Novikovskii, A.A. Novakovich, V.E. Dmitrienko, Phys. Rev. B **82**, 205206 (2010)
39. J. Kokubun, A. Watanabe, M. Uehara, Y. Ninomiya, H. Sawai, N. Momozawa, K. Ishida, V.E. Dmitrienko, Phys. Rev. B **78**, 115112 (2008)
40. V.E. Dmitrienko, E.N. Ovchinnikova, J. Kokubun, K. Ishida, Pis'ma Zh. Eksp. Teor. Fiz. **92**, 424 (2010)
41. V.E. Dmitrienko, E.N. Ovchinnikova, J. Kokubun, K. Ishida, JETP Lett. **92**, 383 (2010)
42. S.P. Collins, et al. (unpublished) (2011)
43. V.E. Dmitrienko, V.A. Chizhikov, Phys. Rev. Lett. **108** (2012) (accepted)
44. Y. Tanaka, T. Takeuchi, S.W. Lovesey, K.S. Knight, A. Chainani, Y. Takata, M. Oura, Y. Senba, H. Ohashi, S. Shin, Phys. Rev. Lett. **100**, 145502 (2008)
45. Y. Tanaka, T. Kojima, Y. Takata, A. Chainani, S.W. Lovesey, K.S. Knight, T. Takeuchi, M. Oura, Y. Senba, H. Ohashi, S. Shin, Phys. Rev. B **81**, 144104 (2010)
46. Y. Kousaka, H. Ohsumi, T. Komesu, T. Arima, M. Takata, S. Sakai, M. Akita, K. Inoue, T. Yokobori, Y. Nakao, E. Kaya, J. Akimitsu, J. Phys. Soc. Japan **78**, 123601 (2009)
47. Y. Tanaka, S.P. Collins, S.W. Lovesey, M. Matsumami, T. Moriwaki, S. Shin, J. Phys. Condens. Matter **22**, 122201 (2010)
48. Y. Tanaka, Eur. Phys. J. Special Topics **208**, 67 (2012)
49. A. Kirfel, J. Grybos, V.E. Dmitrienko, Phys. Rev. B **66**, 165202 (2002)
50. S.P. Collins, D. Laundy, V.E. Dmitrienko, D. Mannix, P. Thompson. Phys, Rev. B **68**, 064110 (2003)
51. G. Beutier, S.P. Collins, G. Nisbet, E.N. Ovchinnikova, V.E. Dmitrienko Eur. Phys. J. Special Topics **208**, 53 (2012)

52. E.N. Ovchinnikova, V.E. Dmitrienko, A.P. Oreshko, G. Beutier, S.P. Collins. J. Phys. Condens. Matter **22**, 355404 (2010)
53. Y. Murakami, J.P. Hill, D. Gibbs, M. Blume, I. Koyama, M. Tanaka, H. Kawata, T. Arima, Y. Tokura, K. Hirota, Y. Endoh, Phys. Rev. Lett. **81**, 582 (1998)
54. G. Subías, J. Herrero-Martín, J. García, J. Blasco, C. Mazzoli, K. Hatada, S. Di Matteo, C.R. Natoli, Phys. Rev. B **75**, 235101 (2007)
55. J. García, G. Subías, J. Phys. Condens. Matter **16**, 145 (2004)
56. E. Nazarenko, J.E. Lorenzo, Y. Joly, J.L. Hodeau, D. Mannix, C. Marin, Phys. Rev. Lett. **97**, 056403 (2006)
57. J.E. Lorenzo, C. Mazzoli, N. Jaouen, C. Detlefs, D. Mannix, S. Grenier, Y. Joly, C. Marin, Phys. Rev. Lett. **101**, 226401 (2008)
58. V. Scagnoli, U. Staub, Y. Bodenthin, R.A. de Souza, M. García-Fernández, M. Garganourakis, A. T. Boothroyd, D. Prabhakaran, S.W. Lovesey, Science **332**, 696 (2011)
59. H.C. Walker, F. Fabrizi, L. Paolasini, F. de Bergevin, J. Herrero-Martin, A.T. Boothroyd, D. Prabhakaran, D.F. McMorrow, Science **333**, 1273 (2011)
60. P.D. Hatton, S.B. Wilkins, T.A.W. Beale, T.K. Johal, D. Prabhakaran, A.T. Boothroyd, J. Sync. Rad. **12**, 434 (2005)